Bone Reports 19 (2023) 101720

Contents lists available at ScienceDirect

Bone Reports

journal homepage: www.elsevier.com/locate/bonr

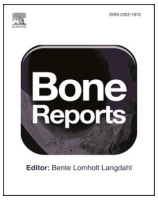

Evaluation of cortical bone remodeling in canines treated with daily and weekly administrations of teriparatide by establishing AI-driven morphometric analyses and GIS-based spatial mapping

Marie Hoshi-Numahata [a,b], Aya Takakura [c,*], Atsuko Nakanishi-Kimura [a,b], Haruhisa Watanabe [a,d], Kentaro Takada [e], Mai Nishiura [a,f], Yoshiaki Sato [b], Ryoko Takao-Kawabata [c,*], Tadahiro Iimura [a,*]

[a] Department of Pharmacology, Faculty and Graduate School of Dental Medicine, Hokkaido University, N13 W7, Sapporo 060-8586, Japan
[b] Department of Orthodontics, Faculty and Graduate School of Dental Medicine, Hokkaido University, N13 W7, Sapporo 060-8586, Japan
[c] Pharmaceuticals Research Center, Asahi Kasei Pharma Corporation, 632-1 Mifuku, Izunokuni, Shizuoka 410-2321, Japan
[d] Department of Oral Medicine and Diagnostics, Faculty and Graduate School of Dental Medicine, Hokkaido University, N13 W7, Sapporo 060-8586, Japan
[e] Department of Natural History Sciences, Graduate School of Science, Hokkaido University, N10 W8, Sapporo 060-8010, Japan
[f] Department of Dentistry for Children and Disabled Persons, Faculty and Graduate School of Dental Medicine, Hokkaido University, N13 W7, Sapporo 060-8586, Japan

ARTICLE INFO

Keywords:
Teriparatide
PTH
Cortical bone
Haversian canal
Artificial intelligence
Geographical information system

ABSTRACT

Larger animal models with a well-developed Haversian system, as observed in humans, are ideal to analyze cortical bone remodeling in pharmacological studies of anti-osteoporosis drugs, although they have some limitations in controlling individual variability in size, weight, age, and number. This study aimed to morphometrically analyze cortical bone remodeling focusing on Haversian canals in dogs using four regimens of TPTD with daily and weekly administrations at lower and higher weekly doses (4.9 μg/kg/week and 19.8 μg/kg/week, respectively) for 9 months. A micro-computed tomography-based analysis showed no significant differences among regimen groups. By establishing artificial intelligence (AI)-driven morphometric analyses and geographical information system (GIS)-based spatial mapping of Haversian canals that does not require confocal microscopy but is possible with more commonly used wide field microscopes, we successfully observed significant morphometric distinctions among regimens applied even in dogs. Our analytical results suggested that the daily higher regimen specifically increased the number of eroded pores creating spaces between existing canals, thus stimulating cortical bone remodeling.

1. Introduction

The dynamic equilibrium of bone resorption and bone formation maintains bone mass and form in healthy adult skeletons. Osteoporosis is an imbalanced condition of bone-resorptive osteoclastic activity that outweighs the bone-forming osteoblastic activity caused by aging, loss of sex hormones, inflammatory diseases, and disuse syndrome, and which therefore increases the risk for bone fracture (2001). Bone fractures, especially in the lumbar vertebrae and femoral neck, are highly associated with a reduction in quality of life and an acute increase in the osteoporotic population, especially in aging societies, which places significant burdens on healthcare systems. Therefore, the prevention and treatment of osteoporosis is an important healthcare issue for maintaining social activity.

Common bone sites of osteoporotic fracture, such as the hip, wrist, and lumbar vertebrae, have been assessed both in preclinical (animal models) and clinical studies, including the pharmacological evaluation of anti-osteoporotic drugs. Both trabecular and cortical bone are important determinants of bone strength, and it is well established that thinner trabeculae and cortices are associated with the risk of vertebral and nonvertebral (appendicular bone) fractures, respectively (Bala et al., 2015; Diab et al., 2006; Shigdel et al., 2015; Stein et al., 2013; Yeni et al., 1997; Zebaze et al., 2010). In fact, the appendicular skeleton is composed of cortical bone, which undergoes significant loss with aging

* Corresponding authors.
E-mail addresses: shimomura.ac@om.asahi-kasei.co.jp (A. Takakura), takao.rb@om.asahi-kasei.co.jp (R. Takao-Kawabata), iimura@den.hokudai.ac.jp (T. Iimura).

https://doi.org/10.1016/j.bonr.2023.101720
Received 3 September 2023; Received in revised form 4 October 2023; Accepted 9 October 2023
Available online 12 October 2023

(Bala et al., 2015; Diab et al., 2006; Stein et al., 2013). Accordingly, 80 % of all fractures occur at sites of weakened, thinned cortical bone (Shigdel et al., 2015; Yeni et al., 1997), and cortical bone porosity is associated with the reduced mechanical strength of bone and a decreasing capacity of bone to absorb impact (Harrison and Cooper, 2015; Harrison et al., 2020).

Despite the relevance of assessing the microarchitecture of cortical bone, the evaluation of the structure of trabecular bone has appeared to dominate the research, which is often described as having a "trabeculocentric" view of bone loss (Bala et al., 2015; Harrison et al., 2020). This is possibly because trabecular bone exhibits more dynamic, morphometrically recognizable and assessable structural changes both in preclinical and clinical studies, while changes in the microarchitecture of the cortices are below the resolution of many imaging modalities. Furthermore, this is also related to the fact that model animals that are commonly used in bone preclinical studies (e.g.), mice and rats show little cortical turnover with few typical structures of osteons throughout their lives, although the cortical bone in larger vertebrates, including humans, exhibits obvious biological turnover (cortical bone remodeling). The remodeling of cortical bone largely takes place on the bone surfaces of Haversian canals that encase neuronal-vascular bundles that compose a central structure of the osteon (Frost, 1969; Hattner et al., 1965; Parfitt, 1982, 1994). An individual remodeling event is regulated by so-called multicellular units (BMUs) that couple and balance bone resorption and formation by osteoclasts and osteoblasts, respectively (Lassen et al., 2017). An imbalance in cortical remodeling with dominant bone resorption over bone formation results in pathological stimulation of cortical bone remodeling, eventually causing an increase in cortical porosity observed in osteoporotic bone (Bjornerem, 2016; Harrison et al., 2020). Therefore, there is an increasing need for innovative assessments of cortical architecture with the spatiotemporal regulation of BMUs in larger animal models of remodeling with a well-developed Haversian system in their cortices.

Teriparatide [TPTD; human parathyroid hormone, hPTH (1–34)] is a bone anabolic drug that is clinically used for the treatment of osteoporosis. The pharmacological effects of TPTD stimulate both bone formation and resorption, thus stimulating bone turnover. Importantly, the intermittent administration of TPTD enhances bone formation such that it exceeds bone resorption, thereby increasing net bone mass, while the continuous administration of TPTD reduces bone mass by stimulating bone resorption over bone formation.

Three distinct regimens (once daily, once weekly, and twice weekly) of TPTD are clinically available for anti-osteoporosis treatment and are known to have some differences in terms of clinical use and pharmacological effects. The once-daily regimen leads to marked increases in both markers of bone formation and resorption, while the once-weekly and twice-weekly regimens show less stimulation of bone resorption (Inoue, 1985; McClung et al., 2005; Shiraki et al., 2013; Sugimoto et al., 2019). The risk reduction effects of vertebral fractures in these distinct regimens appear to be comparable. However, the accumulation of both clinical (Zebaze et al., 2017) and preclinical studies (Hirano et al., 2000a; Hirano et al., 1999; Takakura et al., 2017; Yamane et al., 2017) has demonstrated that distinct administration frequencies, as well as dosing of TPTD, differentially affected the strength of bone due to distinct effects on cortical bone remodeling. Therefore, these three distinct regimens were selected based on the requirements and clinical conditions of each patient.

To evaluate the pharmacological effects of distinct regimens of TPTD on cortical bone remodeling, we previously observed that a high frequency of TPTD administration (6 μg/kg three times daily) in a rat ovariectomized postmenopausal osteoporosis model was associated with the significant development of cortical porosity in vertebral bones, which was associated with increased bone resorption, (Takakura et al., 2017). However, lower frequency administrations (such as 30 μg/kg once daily and 30 μg/kg three times weekly) were not associated with such pathological effects. Subsequent studies in rabbit femurs reported that the frequent administration of TPTD (40 μg/kg once daily) induced a significantly higher score of cortical porosity and the significant expansion of the osteocytic lacunar-canalicular network in comparison to relatively lower-frequency administration regimens (140 μg/kg twice weekly, 280 μg/kg once weekly), even though the total weekly doses of these three regimens were equivalent (Takakura et al., 2022). These preclinical findings suggest that distinct TPTD administration regimens differentially affect cortical bone remodeling and indicate the need for further preclinical studies using a larger animal that has a more similar bone microstructure and turnover rate to those in humans to extrapolate preclinical findings to the clinical setting.

Larger animal models with a well-developed Haversian system in their cortices (as observed in humans), including rabbits, sheep, goats, dogs, and swine, have been employed in research on bone pathophysiology (Jee and Yao, 2001; Reinwald and Burr, 2008; Thompson et al., 1995; Turner, 2001). We herein focus on dogs, which show well-defined cortical remodeling and bone turnover rates similar to those of humans (Boyce et al., 1996), and which are known to respond to parathyroid hormone (PTH) treatment with elevated remodeling and cortical porosity that were observed by iliac bone and rib biopsies (Inoue, 1985). The primary objective of this study was to morphometrically characterize cortical bone remodeling focusing on Haversian canals by providing artificial intelligence (AI)-driven morphometric analyses and geographical information system (GIS)-based spatial mapping in dogs using four regimens of TPTD with daily and weekly administration at lower and higher weekly total doses (4.9 μg/kg/week and 19.8 μg/kg/week, respectively) that were designed as preclinical and toxicity tests. We analyzed cortical bone remodeling of dog rib as a representative specimen to investigate pharmacological effects on cortical bone remodeling and mechanical properties as previously reported(Hirano et al., 2000b; Komatsubara et al., 2004; Mashiba et al., 2000; Wilson et al., 1998), which is supported by clinical findings that spontaneous rib fractures can occur due to severe cough and are more likely to occur in those with osteoporosis(Katrancioglu et al., 2015).

2. Materials and methods

2.1. Animals and the preparation of bone specimens

Fifteen male beagle dogs (TOYO Beagle) were purchased from Kitayama Labes (Nagano, Japan) and allowed to acclimatize with ad libitum access to water and 300 g/day of food (DS-A, Oriental Yeast Co. Ltd., Tokyo, Japan) for two months before use. Throughout the experimental study, the animals were housed individually in concrete - stainless steel cages (78 W × 90 D × 95H cm) under a 12-h light/dark cycle with ad libitum access to water and 300 g/day of food (DS-A, Oriental Yeast, Tokyo, Japan). Both animal care staff and those who administer treatments monitored the animals twice daily. Health was monitored by weight (twice weekly), food intake, and general assessment of animal activity. Animals with a body weight of 7.9–11.3 kg at seven to eight months of age were randomized into five groups (3 animals each) and were subcutaneously injected with 0.7 or 2.8 μg/kg TPTD (Asahi Kasei Pharma Corporation, Tokyo, Japan) once daily (DL group and DH group) or 4.9 or 19.8 μg/kg TPTD once weekly (WL group and WH group) for nine months (Fig. 1, Table 2, Supplementary Fig. 1a). Saline injections were administered to control animals (CNT group) once daily. We planned to exclude any individual animal that showed severe weight loss or other poor conditions from which recovery was not expected during the treatment period, but no such cases occurred. After the dosing period, the animals were euthanized by exsanguination under anesthesia using thiopental. The right ribs were packed in plastic bags and stored at −30 °C until use in microcomputed tomography (CT) imaging, while the left ribs were fixed in 70 % ethanol, stained with Villanueva bone stain, dehydrated in a graded ethanol series, defatted in acetone, and embedded in polymethyl methacrylate (Wako Pure Chemical Industries, Osaka, Japan) (Supplementary Fig. 1b). Thin

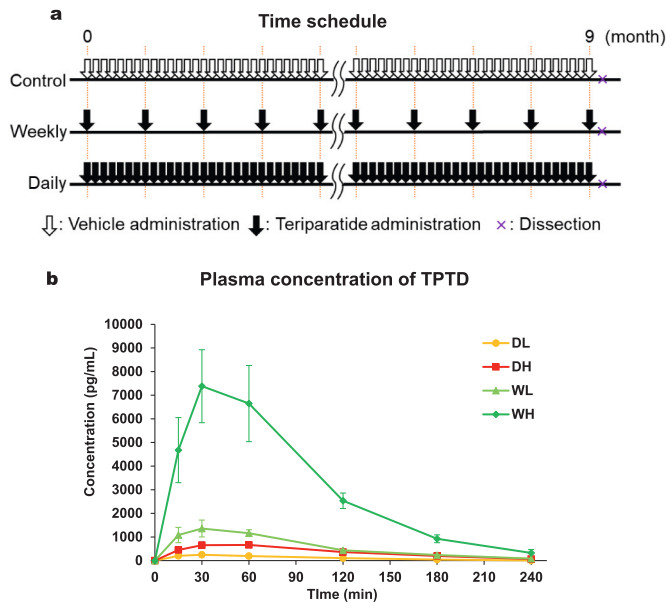

Fig. 1. The time schedule of teriparatide (TPTD) administration and plasma concentration of TPTD. (a) Animals were randomized into five groups: daily low dose (DL) group, daily high dose (DH) group, weekly low dose (WL) group, and weekly high dose (WH) group. Saline injections were administered to control (CNT) group animals once daily for the same period. The details of the dosing regimens of each group are shown in Table 1. (b) The plasma concentration of TPTD. Data are shown as the mean ± SD. The pharmacokinetic parameters of plasma TPTD are shown in Table 2.

ground sections (thickness: 10–20 μm) were prepared using a microcutting machine and a grinding machine (EXAKT, Germany) from a cross-section in a plane of the central rib and were subjected to bone histomorphometry. The experimental protocols were approved by the experimental animal ethics committee at the Asahi Kasei Pharma Corporation and were conducted in accordance with the guidelines for the management and handling of experimental animals. Animals were housed under nonspecific pathogen-free conditions at Ina Research Inc., accredited by AAALAC (The Association for Assessment and Accreditation of Laboratory Animal Care International). Animal care staff and those who administered treatments were not involved in sample measurements. All sample measurements were performed by objective methods.

2.2. Blood sampling for measurement of the plasma TPTD concentration

Blood samples were collected from the veins of the forelimb at 15 and 30 min and 1, 2, 3 and 4 h after the initial administration of TPTD on day 1 (in the TPTD dosing groups). The samples were centrifuged at 1600 xg at 4 °C for 10 min, and plasma samples were collected. The plasma samples were stored at −80 °C until measurement of the TPTD concentration. Teriparatide acetate was synthesized at Asahi Kasei Pharma Corporation (Tokyo, Japan) and was used as a standard substance. The teriparatide acetate concentration in the plasma was quantified using a Rat PTH IRMA Kit (Immutopics, Inc., San Clemente, CA) according to the manufacturer's instructions. The pharmacokinetic parameters were calculated using Phoenix WinNonlin (Pharsight, Mountain View, CA, USA).

2.3. Micro-computed tomography (micro-CT) imaging, and measurement of the bone mineral density

A cone-beam X-ray microfocus CT system (ScanXmate-RB090SS150; Comscantecno, Kanagawa, Japan) was used to obtain micro-CT images of the femoral trochanter and the right ribs using the following settings: tube voltage, 70 kV; tube current, 100 mA; and resolutions of the right ribs and the femoral trochanter, 12.5 μm/voxel and 65.6 μm/voxel, respectively. Three-dimensional images were reconstructed and analyzed using the TRI/3D-BON software program (RATOC System Engineering, Tokyo, Japan). We analyzed regions of the central ribs (2.5 mm in the longitudinal direction) and the femoral trochanter (1 mm of the distal 3–4 mm of the femoral neck branch). The cortical bone structure in the ribs was determined in the samples, and the following parameters were measured: cortical thickness (Ct.Th, μm), cortical bone ratio (cortical volume (Ct.V)/total volume (Tt.V), %), cortical porosity (void volume (Vd.V)/cortical volume (Ct.V), %), internal length (In. L), and external length (Ex.L). The trabecular bone structure was determined in the samples, and the trabecular bone volume (BV/TV) were measured.

Bone mineral densities (BMD) of the collected 4th lumber vertebrae (LV4) were monitored using dual-energy X-ray absorptiometry (DXA) (DCS-600EX-IIIR, Aloka, Tokyo, Japan). The whole samples were scanned at a pitch of 2 mm. The BMD (mg/ cm^2) was then calculated from the bone mineral content (mg) and bone area (cm^2).

2.4. Wide field differential interference contrast (DIC) and fluorescence imaging

Undecalcified bone sections stained by Villanueva bone staining were imaged using a differential interference contrast microscope system, NI-E Microscope (Nikon) and objective lens, Plan Apo λ10× (numerical aperture [NA] = 0.45), (Nikon). The TxRed filter set was used for autofluorescence derived from soft tissues. The tiling of fluorescence and DIC images was performed sequentially with a frame size of 1280 × 1024 pixels per scan, a color depth of 8 bits, and a pixel size of 0.64 μm. The entire section was imaged comprehensively to obtain large, high-contrast images of the whole section. Image processing was performed using the NIS-Elements AR imaging software program (Nikon, Tokyo, Japan).

2.5. Setting of region of interest (ROI) and histomorphometry

Transverse sections of dog ribs simply showed trabecular and cortical structures without much morphological land marks as was observed in long appendicular long bones such as tibias and femurs. Therefore, our morphometrical approaches were conducted separately in trabecular and cortical areas with geometrically defining ROIs as follows to exclude positional bias for analyses. For trabecular bone analyses, a single rectangle covering entire trabecular area was set, and then equally divided in to 3 squares of 1 mm × 1 mm ROI (Supplementary Fig. 2a). For cortical bone analyses, a single square maximally covering cortical bone was first inscribed at the center of each bone section, and then 6 squared ROIs of 400 μm × 400 μm were placed at locations through the vertical midline and two diagonal lines within cortical area (Supplementary Fig. 2b). Morphometric parameters of trabecular bone surface such as bone surface (BS), osteoid volume (OV), osteoid length (OL), and osteoid width (O.Wi) were set as depicted in (Supplementary Fig. 3 a). The parameters that were measured in this study basically followed the standard normal nomenclature(Dempster et al., 2013).

2.6. Artificial intelligence (AI)-driven bone histomorphometry

AI-driven bone histomorphometry of Haversian canals (H·Ca) in cortical bone was performed using AI deep learning methods by imaging analysis tools: NIS-Elements AR and NIS, ai (Nikon) which is commercially available software. As shown in Fig. 4a and S.Fig. 4a, we first prepared “Teaching data” of 3 to 12 different images in which HVCs were manually recognized. Machine learning was performed 1000 times by using the function: “segment. ai” which is included in the software. The AI-learning curve shows that the training loss was sufficiently reduced as the training times increased (S.Fig. 4b). The AI-training data

were applied to the raw data and automatically binarized by AI (Fig. 4b). All obtained images were checked by researchers. Insufficient recognition of HVC was manually corrected. Using this AI-driven morphometric measurement, the following parameters were measured semi-automatically: Object Number, Object area, Length, Width, Perimeter, Smoothness, and Circularity, and these results were analyzed statistically. For bone histomorphometry of the osteoid and bone marrow area, the "Binary Editor" function of the software program was used for manual recognition (manually binarization) and to obtain the following parameters semiautomatically: Object Number, Object area, Length, Width and Perimeter, and these results were analyzed statistically.

2.7. Geographical information system (GIS)-based mapping of Haversian canals

We applied GIS (Arc Map 10.8.1. and Arc GIS Pro 3.1.1.i Redlands, USA) to spatially map Haversian canals (H.Ca) on whole views of histological sections. The density of H.Ca and the size-based distribution of H.Ca area (percentage of the area occupied by H.CA in a unit) were visually mapped as previously described (Cambra-Moo et al., 2012; Gocha and Agnew, 2016; Mallouchou et al., 2020). For the mapping of the density of H.Ca, we segmented the cortical bone areas into 300 μm × 300 μm squares. Visual mapping was performed based on the number of H.Ca contained within each square. For the mapping of the size-based distribution of H.Ca, we used squares of 100 μm × 100 μm as unit. The percentage of H.Ca area within each unit was calculated and visually mapped.

2.8. Statistical analysis

We first conducted Q-Q plots for all data to see whether or not data were considered to follow Gaussian distribution (shown in supplementary Figs. 11–13). For analyses with multiple ROIs per specimen (shown in Fig. 5 and sFig. 3), the Friedman test was performed, and Dunn's multiple comparison test was used for post hoc analysis. All other data were analyzed using Kruskal-Wallis test and then Dunn's multiple comparison test was used for the post hoc analysis. All statistical tests were performed using Graph Pad Prism version 10.0.2, following its Statistics Guide. All data are presented as the mean ± standard deviation (SD). Statistical significance was defined as $p < 0.05$.

3. Results

3.1. Pharmacodynamics of TPTD in dogs

We set four regimens for the 9-month administration of TPTD to dogs: daily low: DL (0.7 μg/kg: 4.9 μg/kg/week) and daily high: DH (2.8 μg/kg: 19.8 μg/kg/week), weekly low: WL (4.9 μg/kg: 4.9 μg/kg/week) and weekly high: WH (19.8 μg/kg: 19.8 μg/kg/week) (Fig. 1a, Table 1, Supplementary Fig. 1a). The plasma concentrations and pharmacokinetic parameters of TPTD during the administration of TPTD under four distinct regimens (DL, DH, WL and WH) are shown in Fig. 1b and Table 2. The plasma levels of TPTD rapidly increased after the administration of TPTD in all regimens, reaching a maximum concentration (Cmax) of 255.7 ± 26.7 pg/mL at 40 min post-dose (Tmax), 693.1 ± 83.7 pg/mL at 40 min, 1367.1 ± 349.9 pg/mL at 40 min and 7383.1 ± 1544.0 pg/mL at 30 min, respectively. The plasma TPTD concentrations under four distinct regimens (DL, DH, WL and WH) then declined with a half-life (T1/2) of 49.5 ± 7.8, 58.8 ± 2.4, 51.1 ± 9.0 and 45.5 ± 9.1 min post-dose, respectively. Comparison of AUC(0–240) and AUC(0-∞) values showed that >90 % of the administered TPTD under all of these regimens was depleted by 4 h.

Table 1
Dosing regimen settings of this study.

Group	Treatment	Dose	Frequency	Total dose per week	n
CNT	Vehicle	0 μg/kg	1/day	0 μg/kg	3
DL	TPTD	0.7 μg/kg	1/day	4.9 μg/kg	3
DH	TPTD	2.8 μg/kg	1/day	19.8 μg/kg	3
WL	TPTD	4.9 μg/kg	1/week	4.9 μg/kg	3
WH	TPTD	19.8 μg/kg	1/week	19.8 μg/kg	3

CNT: vehicle control, DL: daily low, DH: daily high, WL: weekly low, WH: weekly high, TPTD: teriparatide.

Cmax and AUC under WH regimens was extremely high in comparison to those observed in clinical use and previous rabbit studies (Burr et al., 2001; Hirano et al., 1999; Yamane et al., 2017). Thus, to see whether or not the TPTD administrations had some toxic effects, we carried out general histopathological examinations on all of the specimens that were used in our current study (Supplementary Table 1). No obvious toxic effects of TPTD were observed in any specimens in kidney. In sternum and femurs, most of specimens administrated by TPTD showed histological findings such as enlarged osteoblasts, increased number of osteoblasts and thickening of trabecular bone in femurs.

We next measured and compared bone mineral density (BMD) of the 4th lumber vertebral bodies, and bone volume/tissue volume (BV/TV) of the femoral trochanters by dual energy X-ray, and micro-CT, respectively (Supplementary Table 2). None of these parameters showed significant differences among groups.

3.2. Microcomputed tomography (micro-CT) analysis of dog ribs

The effects of the 4 different TPTD regimens and vehicle control on the rib bone structure were analyzed by micro-CT (Fig. 2, Supplementary Fig. 1b). Representative 2D grayscale images of transverse sections obtained by micro-CT are shown in Fig. 2a. The morphometric parameters measured on micro-CT were analyzed and statistically compared (Fig. 2b). None of the parameters of cortical thickness (Ct.Th), cortical bone volume (Ct.V/Tt.V), cortical porosity rate (Ct.Po), internal length (In. L) and external length (Ex. L) showed significant differences among groups. We next analyzed the morphometric parameters of sectioned bone sizes (Fig. 2c and d, Supplementary Fig. 1b). None of the parameters of length, width, width/length, marrow volume, marrow volume/bone volume (BV), or marrow volume/total volume (TV) showed significant differences among the groups.

3.3. Histomorphometry of trabecular bone areas

To observe changes in the microarchitecture in entire transverse sections of canine ribs, we conducted tiling of large high-resolution DIC images and deconvolution fluorescence images using wide field microscopy (Fig. 3). Histomorphometry of trabecular bone areas with setting three region of interest (ROI) (Supplementary Fig. 2a) showed no significant differences in BV/TV, osteoid length (O.Le), osteoid thickness (O.Th), and osteoid volume (OV)/TV among the groups, suggesting that no significant effects of TPTD regimens on trabecular bone (Supplementary Fig. 3). However, O.Le/BS in the WH group were significantly reduced compared to those in the DH group, suggesting stimulated trabecular mineralization in the WH group.

3.4. Artificial intelligence (AI)-driven morphometric analysis demonstrated expanded Haversian canals induced by the DH regimen of TPTD

We often observed relatively expanded Haversian and canal pore-like structures, especially in the DH group (indicated by arrowheads in Fig. 3). This observation prompted us to focus on the morphometric analysis of Haversian canals. To ensure comprehensive and unbiased analyses, we established an AI-driven morphometric analysis (Fig. 4, Supplementary Fig. 4) with images acquired by a wide-field fluorescence microscope equipped with DIC that enabled us to simultaneously compare fluorescence and bright field DIC images of the same regions of

Table 2
Pharmacokinetic parameters of plasma TPTD.

Parameters	Units	DL ($N = 3$)			DH (N = 3)			WL (N = 3)			WH (N = 3)		
Cmax	(pg/mL)	255.7	±	26.7	693.1	±	83.7	1367.1	±	341.9	7383.1	±	1544.0
Tmax	(min)	40.0	±	17.3	40.0	±	17.3	40.0	±	17.3	30.0	±	0
AUC (0-240 min)	(ng•min/mL)	25.6	±	2.5	84.4	±	8.4	137.0	±	14.8	720.6	±	106.5
AUC (0-∞)	(ng•min/mL)	26.9	±	1.7	89.9	±	8.0	143.5	±	11.7	743.2	±	97.0
T1/2	(min)	49.5	±	7.8	58.8	±	2.4	51.1	±	9.0	45.5	±	9.1

Cmax: maximum concentration, Tmax: time to maximum concentration, AUC: area under the curve, T1/2: half-life.
All data are shown as the mean ± SD.

interest. We first prepared a set of teaching data that were manually scored for Haversian canals dissociated from osteocytic lacunae with careful observations of bright field DIC and corresponding fluorescence images (Fig. 4a). Machine training was then repeatedly conducted up to 1000 times, achieving a 0.05 % training loss rate (Fig. 4a, b, Supplementary Fig. 4b). To conduct AI-driven morphometric analysis, AI-driven binarization of fluorescence signals derived from Haversian canals was performed (Fig. 4b). When insufficient recognition of a fluorescence signal was noticed, we manually corrected the recognition (Steps 2 and 3 in Fig. 4b). This approach successfully achieved the automatic recognition of Haversian canals that could not be reached by conventional binarization based on light intensity (Fig. 4c).

Based on this AI-driven recognition of Haversian canals of fluorescence images (Fig. 5), we set the parameters of osteoid volume and length in Haversian canals (Fig. 5a). We then statistically compared four parameters of BV/TV, number of Haversian canals (H.Ca), mean area of H.Ca and total area of H.Ca with obtained scores from single ROI of whole cortical bone per specimen (Supplementary Fig. 6). None of these parameters did not show any significant differences among the groups. Histograms of pore size distributions indicated that the number of Haversian canals larger than 2000 μm^2 were obviously increased in the DH group (Supplementary Fig. 7, indicated by a red arrow), suggesting that only a small fraction of the canals, possibly a population of actively remodeling pores, was stimulated by the TPTD administration. We also noticed that relatively enlarged Haversian canals appeared to be located in the middle layer, not outer and inner layers, of cortical bone (Fig. 3), suggesting region-specific response to TPTD as we previously observed in rabbit tibiae(Takakura et al., 2022). We next set six ROIs per specimen with unbiased manner in the middle layer (Supplementary Fig. 2b). Based on this ROI setting, the BV/TV value in the DH group was significantly reduced in comparison to that in the control group (Fig. 5b). The mean and total areas of H.Ca were significantly expanded in the DH group in comparison to those in the control group, although the number of H.Ca did not show any significant difference.

To confirm this analysis, we applied the AI-driven recognition of Haversian canals to bright field DIC images (Fig. 5c, Supplementary Figs. 4, 5). BV/TV in the DL, DH, WL and WH groups was significantly reduced in comparison to that in the control group. Consistent with the BV/TV data, the mean and total area of H.Ca in the DL, DH, WL and WH groups were significantly expanded in comparison to that in the control group. These bright filed image-based analyses showed that the mean and total areas of H.Ca were most significantly expanded in the DH group in comparison to those in the control group. These findings indicated that both AI-driven recognition of Haversian canals applied to fluorescence and bright field images showed the same tendencies in the analyzed morphometric scores and suggested active bone resorption of Haversian canals, especially in the DH group.

To morphometrically analyze bone remodeling of the Haversian canals, we statistically compared the parameters of the osteoids (Fig. 5d) with setting six ROIs per specimen. Although the number of H.Ca with Osteoid did not show significant changes, the parameters of osteoid volume/tissue volume (OV/TV) in the DH and WH groups were significantly higher than those in the control group. The mean osteoid length (O.Le) in the DL and DH were significantly higher than that in the control. Consistently, the total O.Le/total H.Ca perimeter (pm) in the DL, DH, and WH groups showed significantly higher scores than that in the control group.

3.5. Eroded pores of Haversian canals were increased by the DH regimen of TPTD

We further scored and statistically compared cortical porosity by defining “eroded pores” that resorb cement lines of adjacent osteons (Fig. 6) (Andreasen et al., 2018). Although the mean area of eroded pores (E.Po) did not show any significant differences, the number of E.Po especially in the DH group, showed significantly higher score than that of the WH group. This score in the DH group was also higher than those in the control, DL and WL, albeit not significantly. Consistently, the total area of E.Po was significantly higher than that in the WH group. Interestingly, these analyses suggested that eroded pores of Haversian canals were significantly increased especially when comparing between the DH and WH groups, whose weekly total doses were set at the same value of 19.8 μg/kg,

3.6. Geographical information system (GIS) mapping of Haversian canals demonstrated fused Haversian canals induced by the DH regimen of TPTD

It is possible that the increased number of the eroded pores is a readout of actively drifting osteons and fused Haversian canals derived from multiple canals, which reduce the density of Haversian canals. To confirm this, we took advantage of a GIS applied to our AI-driven recognition of Haversian canals in whole histological sections (Fig. 7). We spatially mapped the density of Haversian canals (H.Ca) and the ratio of H.Ca area/unit area (shown as the percentage of the H.Ca area) on all histological sections (Fig. 7, Supplementary Figs. 9-12). This spatial mapping demonstrated that areas with reduced H.Ca density tended to coincide with areas with expanded H.Ca, which was most clear in specimens obtained from the DH group. Therefore, the significant increase in the number of the eroded pores in the DH group was suggested to be caused by fused Haversian canals.

4. Discussion

This study was designed to determine whether different doses and frequencies of TPTD administration for a long period of 9 months had different effects on cortical bone remodeling of Haversian canals in dogs. The administration frequencies and duration were set to the same as the clinical use of TPTD, while the higher concentration was set as a toxicity test. The pharmacokinetics of the plasma TPTD levels after the administration of TPTD at four distinct concentrations (0.7 μg/kg, 2.8 μg/kg, 4.9 μg/kg, and 19.8 μg/kg) in dogs showed that Cmax and AUC were associated with the concentrations of TPTD that were administered. However, the plasma TPTD levels appeared to return to the basal levels within 4 h of administration in all dosage regimens. Consistently, T1/2 of all dosages was comparable (<1 h). These findings were very similar to our previous observation of the pharmacokinetics of plasma TPTD levels in rabbits after administration at four distinct doses (20, 40, 140, and 280 μg/kg) (Yamane et al., 2017). A previous study by Frolik et al.

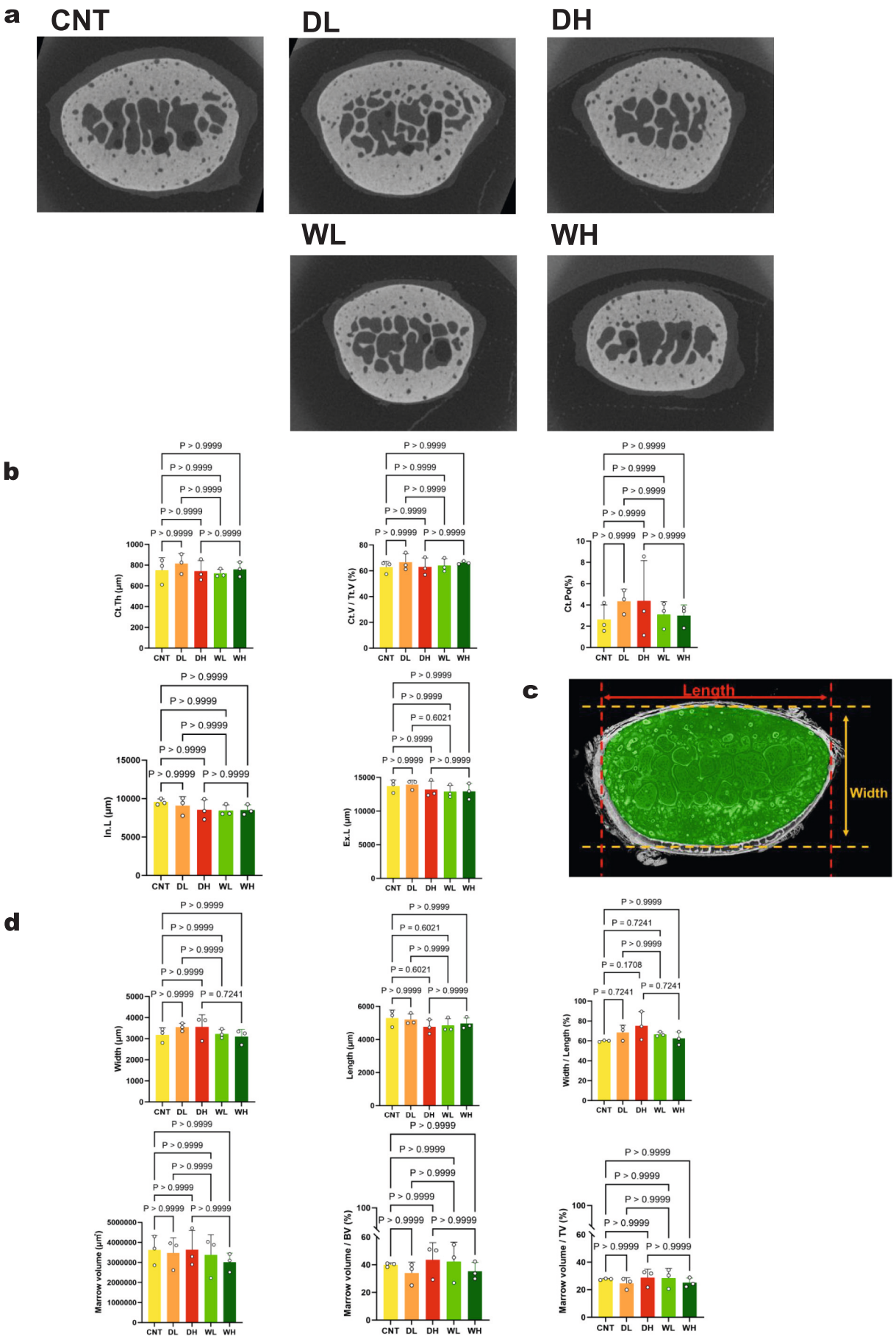

(caption on next page)

Fig. 2. The micro-CT analysis of the cortical bone of the right ribs. (a) Micro-CT images of each group. (b) Ct.Th: Cortical thickness, Ct.V/Tt.V: Cortical volume/total volume, Ct.Po: Cortical porosity (Void volume/cortical volume), In. L: Internal Length, Ex. L: external length. (c) The figure demonstrates the method of measurement used to obtain data shown in Fig. 2d. The long axis of the section of the bone specimen was defined as the length, and the short axis was defined as the width. (d) Morphometric parameters of sectioned bone sizes. We measured the length, width, width/length, marrow volume, marrow volume/BV, and marrow volume/TV. All data are shown as the mean ± SD. These data were analyzed by using Kruskal-Wallis test and there are no significant difference among each groups. ($n = 3$ dogs).

with several TPTD dosage regimens in rat models demonstrated that the duration for which the serum level of TPTD was elevated was a primary determinant of the anabolic and catabolic effects on bone mass, while the magnitude of the Cmax and AUC values of serum PTH was not correlated with these effects (Frolik et al., 2003). Histopathological analyses did not show obvious toxic effects of TPTD in skeletal and non-skeletal tissues. Therefore, it was hypothesized that any of the administration regimen settings in this study would exert the pharmacological effects of TPTD on bone.

This study used dogs as a model animal to analyze the pharmacological effects of TPTD on cortical bone remodeling. In comparison to commonly used small animal models such as mice and rats, dogs are expected to provide ideal large animal models to extrapolate pharmacological responses to human studies because their Haversian

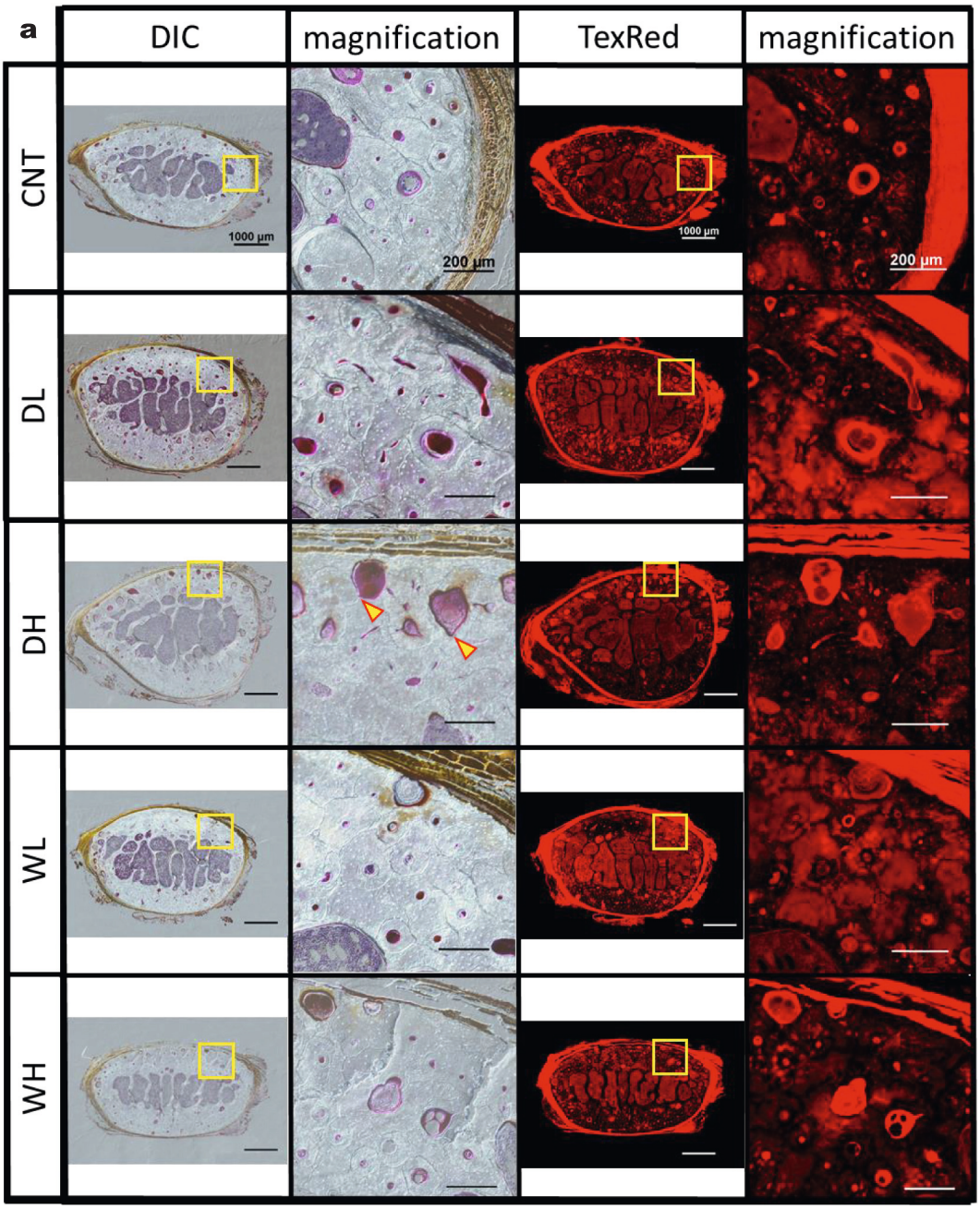

Fig. 3. Differential interference contrast (DIC) and fluorescence images of dog rib sections of each group. Representative bone specimens in each CNT, DL, DH, WL, and WH group are shown. Magnified views of the sites indicated by yellow rectangles in each whole view are shown. Yellow arrowheads surrounded by red indicate rough bone surfaces demarcating the active bone resorption of Haversian canals. The scale bars are 1000 μm and 200 μm in whole and magnified images, respectively.

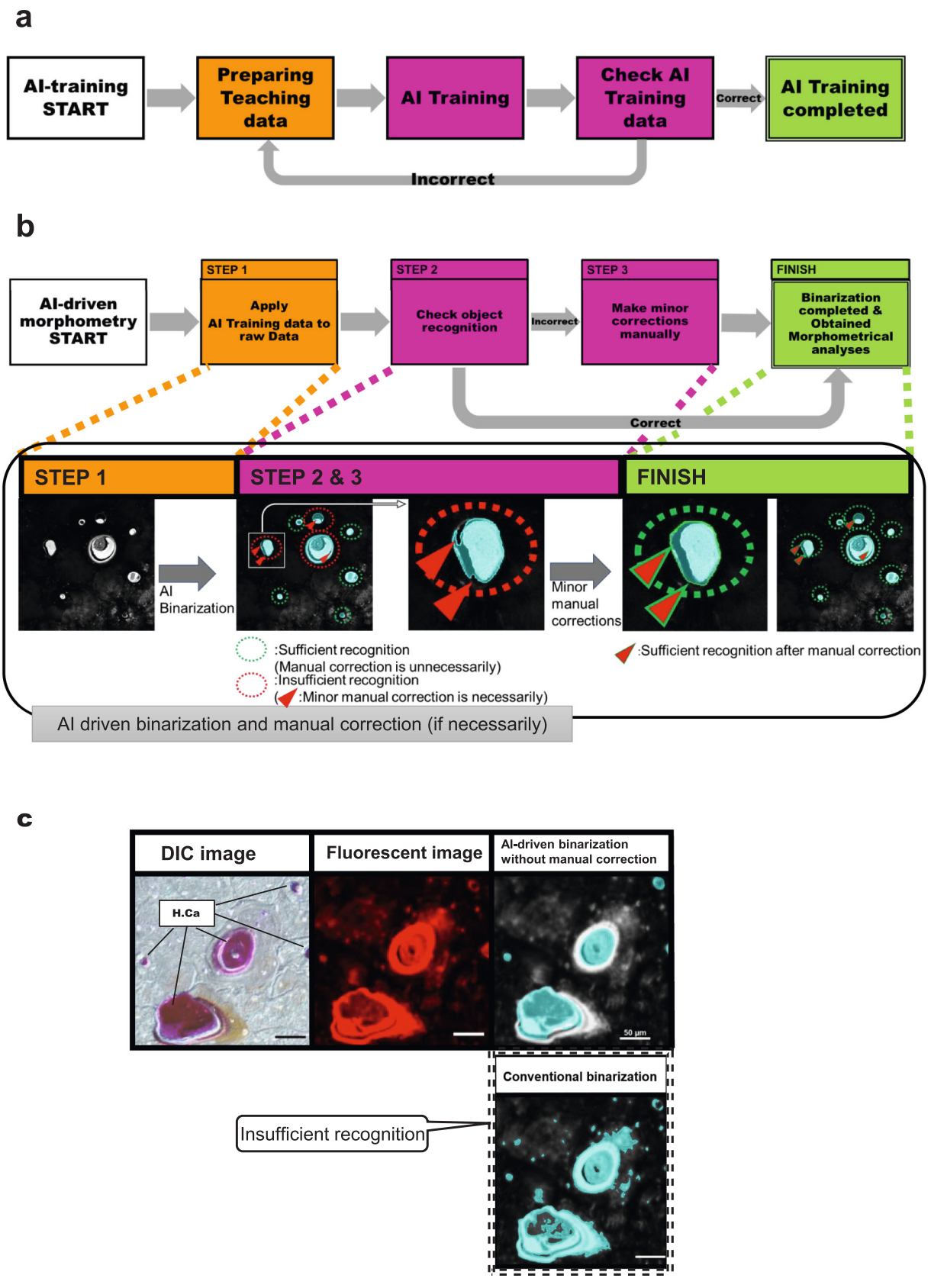

Fig. 4. Methodological flow charts of AI-driven bone histomorphometry. (a) Flow chart of AI training. (b) Flow chart of AI-driven object binarization with or without minor manual correction. (c) Comparison chart of AI-driven binarization and conventional binarization. The binarized objects are highlighted in blue.

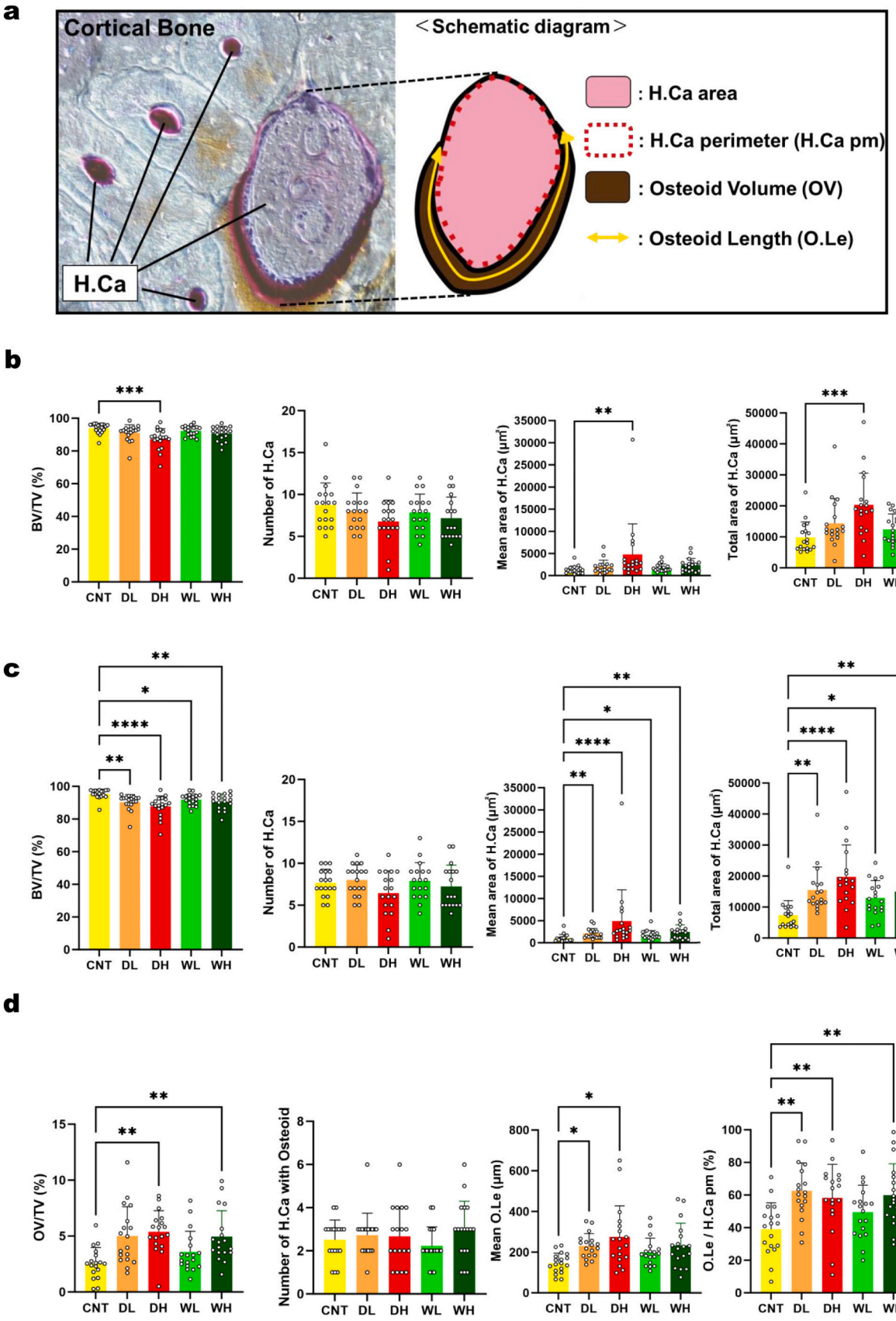

Fig. 5. The bone morphometric analysis using wide-field fluorescence and DIC images in cortical bone. (a) Schematic diagram showing the parameter settings of the morphometric analysis. (b) The results of fluorescence image-derived parameters related to H.Ca. (c) The results of bright field-derived parameters related to H.Ca. (d) The results of parameters related to osteoids. All data are shown as the mean ± SD. Significant differences were determined using Friedman test and then Dunn's multiple comparisons test was used for the post hoc analysis. (*: $P < 0.05$, **: $P < 0.01$, ***: $P < 0.001$, ****:$P < 0.0001$) ($n = 6$ ROIs × 3 dogs =18).

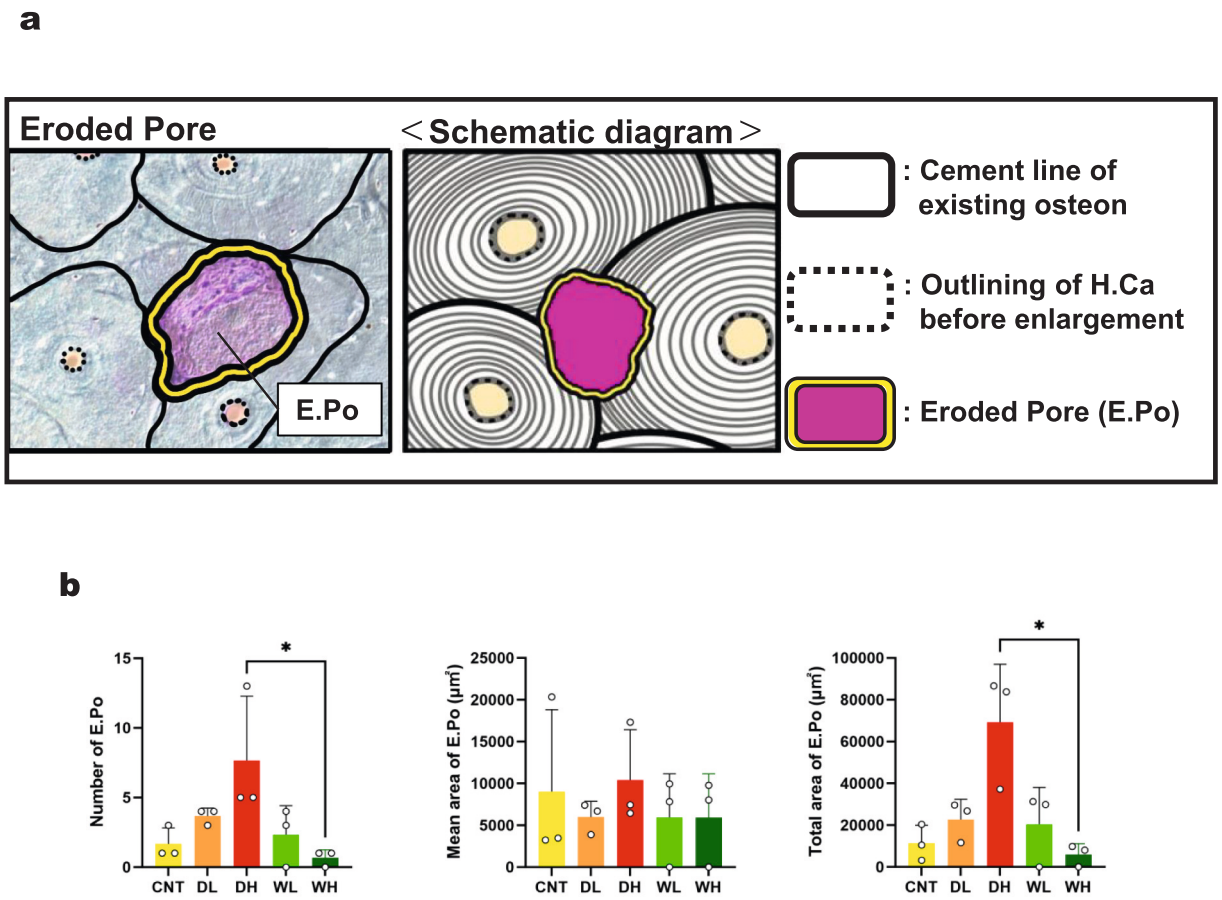

Fig. 6. The quantitative analysis of eroded pores (E.Po) in cortical bone. (a) A schematic diagram of E.Po. E.Po were defined as pores that absorbed the surrounding osteons. (b) The analysis of E.Po. The number, mean area, and total area are shown. All data are shown as the mean ± SD. Significant differences were determined using Krukal-Wallis test and then Dunn's multiple comparisons test was used for the post hoc analysis. (*: $P < 0.05$) ($n = 3$ dogs).

remodeling and the density of osteons in long bones match those of humans (Reinwald and Burr, 2008). The remodeling cycles in dogs are ~25 % shorter than those in humans, and the cancellous turnover rate is two to three times that in humans (Boyce et al., 1996). Despite some similarities between human and dog bone, there are some concerns and uncertainties in studies on bone metabolism in dogs. One is because the ovariectomy does not always accurately recapitulate the post-menopausal osteoporosis due to the uncertainness of the menopausal cycle and dietary calcium intake(Reinwald and Burr, 2008). Second is because the age range often has to be wide, and the numbers in experimental groups are often small due to the difficulty in expansion of breeding. Nevertheless, this study used male dogs to follow up a previous study administrating TPTD for a long period by Inoue(Inoue, 1985), and took advantage of dogs as the abovementioned ideal animal model to investigate the pharmacodynamics and toxicity as well as the pharmacological effects of TPTD. Small group size requires very large differences in the use of morphometric endpoints such as BV/TV, and brings concerns in that the site examined may not be representative of the changes in morphometric parameters. Indeed, this is the case with this study. None of the micro-CT-based parameters of rib bones in the small size of the five experimental groups ($n = 3$) showed significant differences (Fig. 1). Neither of the BMD of lumber vertebral bodies nor the BV/TV of trabeculae in femoral trochanters showed significant differences (Supplementary Fig. 1). The body weight and growth rate in each specimen appeared to show individual differences (Supplementary Fig. 1), which might be affected by heterogeneity in the genetic background. By biopsies of dog iliac and rib bones taken before and after the TPTD administration, Inoue previously observed that TPTD administration to male dogs significantly elevated histomorphometric parameters of bone formation as well as bone resorption, but not bone volume of trabeculae and cortices(Inoue, 1985). This study suggested that TPTD was effective in stimulating the bone turnover rate, which could be observed by temporal sampling and comparisons of bones in each dog specimen.

Morphometric analyses and histological measurements of trabecular bone to compare the drug administration groups in this study, however, did not show any significant differences. This was very similar to studies in ovariectomized monkey models to which TPTD was administered for a long period of 24 months, which suggested that bone remodeling did not obviously react to TPTD after long treatment (Yoshitake et al., 2019). Nevertheless, histological observations of cortical bone in this study showed somewhat distinct appearances in the shape of Haversian canals, especially of specimens in the DH group, which prompted us to establish AI-driven morphometric analyses of Haversian canals to comprehensively compare remodeling features of cortical bones with distinct TPTD regimens. This method successfully revealed that the size of Haversian canals was significantly enlarged in the DH group in comparison to other regimen settings (Fig. 5b, c), suggesting increased bone resorption on the surface of Haversian canals, which was supported by the increased number of eroded pores destroying surrounding osteons (Fig. 6b). Furthermore, morphometric analyses based on bright field images of osteoid on the surface of bone encasing Haversian canals showed significantly augmented bone formation in the DL, DH, WL and WH groups, in comparison to the control group. These findings suggested that active bone remodeling in Haversian canals still occurred even after 9 months of TPTD administration.

This study methodologically applied GIS to the AI-driven recognition of Haversian canals. This method spatially mapped whole Haversian

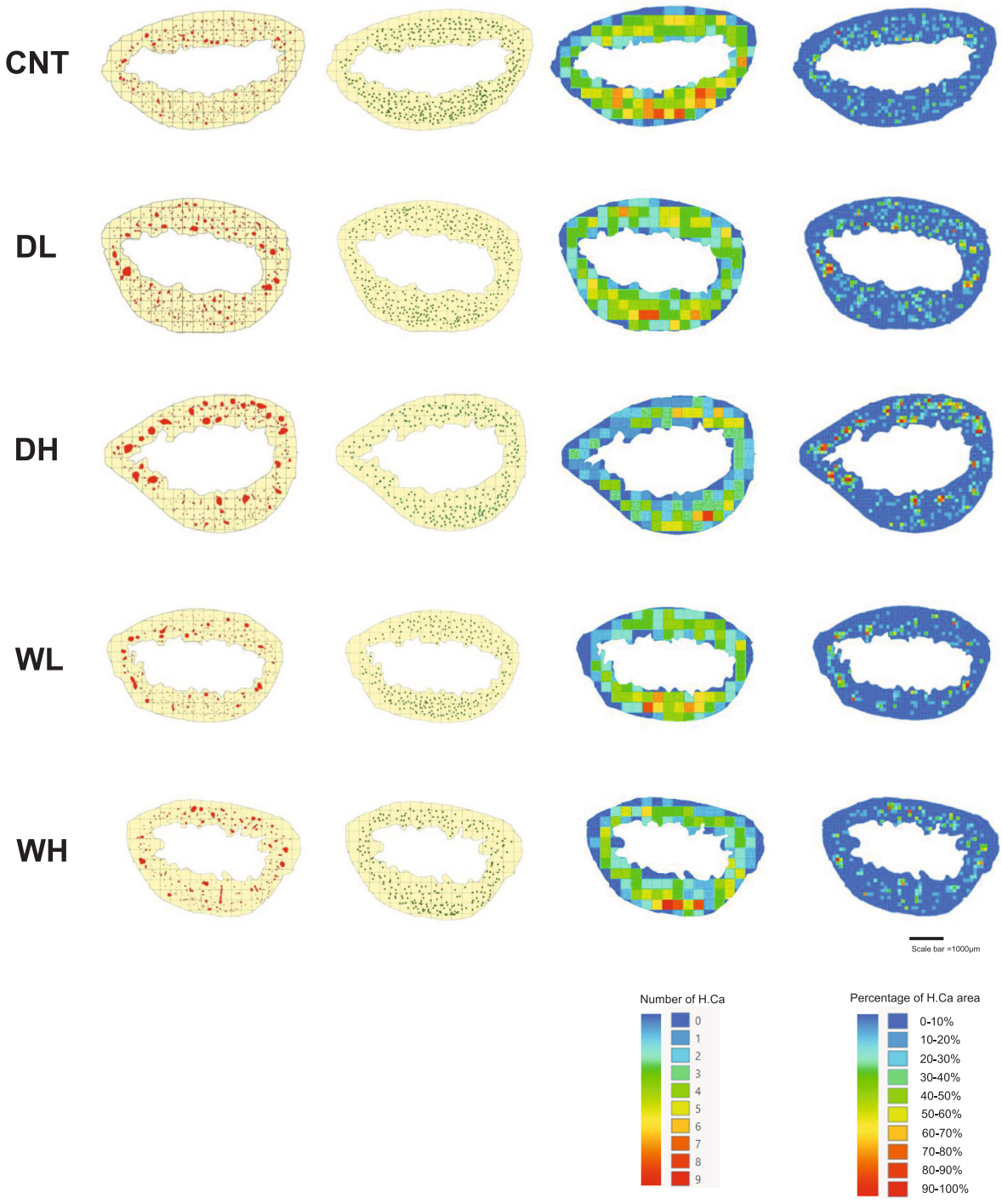

Fig. 7. Spatial mapping of Haversian canals by the GIS method. Mapping of binarized images, center points, density-based distribution and size-based distribution of Haversian canals is shown from left to right. Scale bar = 1000 μm.

canals on bone sections and visually demonstrated the distribution pattern of distinct densities and sizes of Haversian canals. The significant increase in the number of the eroded pores that was observed, especially in the DH regimen, was suggested to be due to active drifting and fusion of canals, in which eroded pores create new spaces between existing canals. Our combined approaches of AI-driven recognition and GIS enabled us to conduct an in-depth study concerning both histo-morphological appearance and histomorphometric estimation of the cortical bone. The spatial visualization and spatial analyses of the morphology of Haversian canals can also provide temporal information on changes in cortical remodeling in response to TPTD. Our analytical method, which did not require confocal microscopy, was implemented with more commonly used wide field microscopy. It was successful in analyzing cortical bone remodeling while overcoming some limitations in the pharmacological application of large animal models such as dogs.

This work has some limitations. The obvious one is the very small sample size (n = 3 dogs in each regimen groups), which may have hindered distinct pharmacological differences by our regimen settings, although some other uncertain factors using dogs could affected statistic comparisons as discussed above. AI algorithms tend to require large sets of appropriate teaching data that still needs some manual efforts especially on morphometrical recognition and segmentation. It is noticeable

that our AI-driven recognition of Haversian canals applied to bright field images unexpectedly brought better statistical resolution than that applied to fluorescence images, which may suggests that not only binarization based on light intensity but also multiple color depth and detailed structural and texture differences can be informative to AI based morphometry. This point should be further investigated for future studies on AI-driven analysis of bone histomorphometry.

In conclusion, the once-daily administration of the higher dose of TPTD for a long period of time (9 months) induced a marked increase in the resorption phases of Haversian canal remodeling and cortical porosity, which were not observed following the once-weekly administration of equivalent total weekly doses. This observation was highly similar to our previous observations using rabbits with three distinct administration frequencies of TPTD: once (1/w), twice (2/w), and seven times (7/w) a week, with the same total dose (140 μg/kg/week) for a short period (1 month). Only a frequent administration regimen (7/w) of TPTD significantly increased the size of Haversian canals accompanied by the development of cortical porosity and endosteal naïve bone formation (marrow fibrosis); however, 1/w and 2/w administration of TPTD showed little effect (Takakura et al., 2022; Yamane et al., 2017). Therefore, long treatment with TPTD, even after an obvious increase in bone mass by TPTD is no longer observed, still shows its pharmacological effects on cortical bone remodeling. The cortical porosity induced by TPTD is potentially driven by both basic multicellular unit (BMU) imbalance (more resorption vs. formation) and/or changes in the rate of cortical bone remodeling (Martin, 1991). Further appropriate long-term clinical studies will be required to improve the treatment of osteoporosis in patients with a high risk of fracture, in whom the porosity of the cortical bone may be increased.

CRediT authorship contribution statement

Marie Hoshi-Numahata: Writing – original draft, Investigation, Formal analysis, Data curation. **Aya Takakura:** Writing – original draft, Investigation, Formal analysis, Data curation, Conceptualization. **Atsuko Nakanishi-Kimura:** Investigation, Formal analysis, Data curation. **Haruhisa Watanabe:** Methodology, Investigation, Formal analysis, Data curation. **Kentaro Takada:** Methodology, Investigation, Formal analysis, Data curation. **Mai Nishiura:** Methodology, Investigation, Formal analysis, Data curation. **Yoshiaki Sato:** Project administration, Data curation. **Ryoko Takao-Kawabata:** Writing – original draft, Supervision, Project administration, Formal analysis, Data curation, Conceptualization. **Tadahiro Iimura:** Writing – original draft, Supervision, Resources, Project administration, Methodology, Funding acquisition, Data curation, Conceptualization.

Declaration of competing interest

A. Takakura and R. Takao-Kawabata are employees of Asahi Kasei Pharma Corporation. The remaining authors declare no conflict of interest.

Data availability

Data will be made available on request.

Acknowledgments

This study was funded by the Asahi Kasei Pharma Corporation. This work was also supported by a Grant-in-Aid for Scientific Research from the Japan Society for the Promotion of Science (JSPS KAKENHI), Grant Number 23K18347 to Tadahiro Iimura. This work was also supported by JST SPRING, Grant Number JPMJSP2119 to M. Hoshi-Numahata, A. Nakanishi-Kimura, H. Watanabe and M. Nishiura.

Appendix A. Supplementary data

Supplementary data to this article can be found online at https://doi.org/10.1016/j.bonr.2023.101720.

References

Andreasen, C.M., et al., 2018. Understanding age-induced cortical porosity in women: the accumulation and coalescence of eroded cavities upon existing intracortical canals is the main contributor. J. Bone Miner. Res. 33 (4), 606–620. https://doi.org/10.1002/jbmr.3354.

NIH consensus development panel on osteoporosis prevention, diagnosis, and therapy, march 7-29, 2000: highlights of the conference. South. Med. J. 94 (6), 2001, 569–573.

Bala, Y., et al., 2015. Role of cortical bone in bone fragility. Curr. Opin. Rheumatol. 27 (4), 406–413. https://doi.org/10.1097/BOR.0000000000000183.

Bjornerem, A., 2016. The clinical contribution of cortical porosity to fragility fractures. Bonekey Rep. 5, 846. https://doi.org/10.1038/bonekey.2016.77.

Boyce, R.W., et al., 1996. Effects of intermittent hPTH(1-34) alone and in combination with 1,25(OH)(2)D(3) or risedronate on endosteal bone remodeling in canine cancellous and cortical bone. J. Bone Miner. Res. 11 (5), 600–613. https://doi.org/10.1002/jbmr.5650110508.

Burr, D.B., et al., 2001. Intermittently administered human parathyroid hormone(1-34) treatment increases intracortical bone turnover and porosity without reducing bone strength in the humerus of ovariectomized cynomolgus monkeys. J. Bone Miner. Res. 16 (1), 157–165. https://doi.org/10.1359/jbmr.2001.16.1.157.

Cambra-Moo, O., et al., 2012. Mapping human long bone compartmentalisation during ontogeny: a new methodological approach. J. Struct. Biol. 178 (3), 338–349. https://doi.org/10.1016/j.jsb.2012.04.008.

Dempster, D.W., et al., 2013. Standardized nomenclature, symbols, and units for bone histomorphometry: a 2012 update of the report of the ASBMR Histomorphometry Nomenclature Committee. J. Bone Miner. Res. 28 (1), 2–17. https://doi.org/10.1002/jbmr.1805.

Diab, T., et al., 2006. Age-related change in the damage morphology of human cortical bone and its role in bone fragility. Bone 38 (3), 427–431. https://doi.org/10.1016/j.bone.2005.09.002.

Frolik, C.A., et al., 2003. Anabolic and catabolic bone effects of human parathyroid hormone (1-34) are predicted by duration of hormone exposure. Bone 33 (3), 372–379. https://doi.org/10.1016/s8756-3282(03)00202-3.

Frost, H.M., 1969. Tetracycline-based histological analysis of bone remodeling. Calcif. Tissue Res. 3 (3), 211–237. https://doi.org/10.1007/BF02058664.

Gocha, T.P., Agnew, A.M., 2016. Spatial variation in osteon population density at the human femoral midshaft: histomorphometric adaptations to habitual load environment. J. Anat. 228 (5), 733–745. https://doi.org/10.1111/joa.12433.

Harrison, K.D., Cooper, D.M., 2015. Modalities for visualization of cortical bone remodeling: the past, present, and future. Front Endocrinol (Lausanne) 6, 122. https://doi.org/10.3389/fendo.2015.00122.

Harrison, K.D., et al., 2020. Cortical bone porosity in rabbit models of osteoporosis. J. Bone Miner. Res. 35 (11), 2211–2228. https://doi.org/10.1002/jbmr.4124.

Hattner, R., et al., 1965. Suggested sequential mode of control of changes in cell behaviour in adult bone remodelling. Nature 206 (983), 489–490. https://doi.org/10.1038/206489a0.

Hirano, T., et al., 1999. Anabolic effects of human biosynthetic parathyroid hormone fragment (1-34), LY333334, on remodeling and mechanical properties of cortical bone in rabbits. J. Bone Miner. Res. 14 (4), 536–545. https://doi.org/10.1359/jbmr.1999.14.4.536.

Hirano, T., et al., 2000a. Changes in geometry and cortical porosity in adult, ovary-intact rabbits after 5 months treatment with LY333334 (hPTH 1-34). Calcif. Tissue Int. 66 (6), 456–460. https://doi.org/10.1007/s002230010091.

Hirano, T., et al., 2000b. Does suppression of bone turnover impair mechanical properties by allowing microdamage accumulation? Bone 27 (1), 13–20. https://doi.org/10.1016/s8756-3282(00)00284-2.

Inoue, J., 1985. Bone changes with long term administration of low dose 1-34 human PTH on adult beagles. Nihon Seikeigeka Gakkai Zasshi 59 (4), 409–427.

Jee, W.S., Yao, W., 2001. Overview: animal models of osteopenia and osteoporosis. J. Musculoskelet. Neuronal Interact. 1 (3), 193–207.

Katrancioglu, O., et al., 2015. Spontaneous rib fractures. Asian Cardiovasc. Thorac. Ann. 23 (6), 701–703. https://doi.org/10.1177/0218492315586485.

Komatsubara, S., et al., 2004. Suppressed bone turnover by long-term bisphosphonate treatment accumulates microdamage but maintains intrinsic material properties in cortical bone of dog rib. J. Bone Miner. Res. 19 (6), 999–1005. https://doi.org/10.1359/JBMR.040126.

Lassen, N.E., et al., 2017. Coupling of bone resorption and formation in real time: new knowledge gained from human Haversian BMUs. J. Bone Miner. Res. 32 (7), 1395–1405. https://doi.org/10.1002/jbmr.3091.

Mallouchou, M., et al., 2020. Mapping Cheshire Cats' leg: a histological approach of cortical bone tissue through modern GIS technology. Anat. Sci. Int. 95 (1), 104–125. https://doi.org/10.1007/s12565-019-00503-4.

Martin, R.B., 1991. On the significance of remodeling space and activation rate changes in bone remodeling. Bone 12 (6), 391–400. https://doi.org/10.1016/8756-3282(91)90028-h.

Mashiba, T., et al., 2000. Suppressed bone turnover by bisphosphonates increases microdamage accumulation and reduces some biomechanical properties in dog rib. J. Bone Miner. Res. 15 (4), 613–620. https://doi.org/10.1359/jbmr.2000.15.4.613.

McClung, M.R., et al., 2005. Opposite bone remodeling effects of teriparatide and alendronate in increasing bone mass. Arch. Intern. Med. 165 (15), 1762–1768. https://doi.org/10.1001/archinte.165.15.1762.

Parfitt, A.M., 1982. The coupling of bone formation to bone resorption: a critical analysis of the concept and of its relevance to the pathogenesis of osteoporosis. Metab. Bone Dis. Relat. Res. 4 (1), 1–6. https://doi.org/10.1016/0221-8747(82)90002-9.

Parfitt, A.M., 1994. Osteonal and hemi-osteonal remodeling: the spatial and temporal framework for signal traffic in adult human bone. J. Cell. Biochem. 55 (3), 273–286. https://doi.org/10.1002/jcb.240550303.

Reinwald, S., Burr, D., 2008. Review of nonprimate, large animal models for osteoporosis research. J. Bone Miner. Res. 23 (9), 1353–1368. https://doi.org/10.1359/jbmr.080516.

Shigdel, R., et al., 2015. Bone turnover markers are associated with higher cortical porosity, thinner cortices, and larger size of the proximal femur and non-vertebral fractures. Bone. 81, 1–6. https://doi.org/10.1016/j.bone.2015.06.016.

Shiraki, M., et al., 2013. Effects of a single injection of teriparatide on bone turnover markers in postmenopausal women. Osteoporos. Int. 24 (1), 219–226. https://doi.org/10.1007/s00198-012-2159-7.

Stein, E.M., et al., 2013. Primary hyperparathyroidism is associated with abnormal cortical and trabecular microstructure and reduced bone stiffness in postmenopausal women. J. Bone Miner. Res. 28 (5), 1029–1040. https://doi.org/10.1002/jbmr.1841.

Sugimoto, T., et al., 2019. Study of twice-weekly injections of Teriparatide by comparing efficacy with once-weekly injections in osteoporosis patients: the TWICE study. Osteoporos. Int. 30 (11), 2321–2331. https://doi.org/10.1007/s00198-019-05111-6.

Takakura, A., et al., 2017. Administration frequency as well as dosage of PTH are associated with development of cortical porosity in ovariectomized rats. Bone Res. 5, 17002. https://doi.org/10.1038/boneres.2017.2.

Takakura, A., et al., 2022. Expansion of the osteocytic lacunar-canalicular system involved in pharmacological action of PTH revealed by AI-driven fluorescence morphometry in female rabbits. Sci. Rep. 12 (1), 16799. https://doi.org/10.1038/s41598-022-20793-5.

Thompson, D.D., et al., 1995. FDA guidelines and animal models for osteoporosis. Bone 17 (4 Suppl), 125S–133S. https://doi.org/10.1016/8756-3282(95)00285-l.

Turner, A.S., 2001. Animal models of osteoporosis—necessity and limitations. Eur. Cell. Mater. 1, 66–81. https://doi.org/10.22203/ecm.v001a08.

Wilson, A.K., et al., 1998. Ovariectomy-induced changes in aged beagles: histomorphometry of rib cortical bone. Calcif. Tissue Int. 62 (3), 237–243. https://doi.org/10.1007/s002239900423.

Yamane, H., et al., 2017. Acute development of cortical porosity and endosteal naive bone formation from the daily but not weekly short-term administration of PTH in rabbit. PloS One 12 (4), e0175329. https://doi.org/10.1371/journal.pone.0175329.

Yeni, Y.N., et al., 1997. The influence of bone morphology on fracture toughness of the human femur and tibia. Bone 21 (5), 453–459. https://doi.org/10.1016/s8756-3282(97)00173-7.

Yoshitake, S., et al., 2019. Once-weekly teriparatide treatment prevents microdamage accumulation in the lumbar vertebral trabecular bone of ovariectomized cynomolgus monkeys. Calcif. Tissue Int. 104 (4), 402–410. https://doi.org/10.1007/s00223-018-0500-7.

Zebaze, R.M., et al., 2010. Intracortical remodelling and porosity in the distal radius and post-mortem femurs of women: a cross-sectional study. Lancet 375 (9727), 1729–1736. https://doi.org/10.1016/S0140-6736(10)60320-0.

Zebaze, R., et al., 2017. Increased cortical porosity is associated with daily, not weekly, administration of equivalent doses of teriparatide. Bone 99, 80–84. https://doi.org/10.1016/j.bone.2017.03.042.